

MAHATMA GANDHI UNIVERSITY
PROJECT REPORT

MODULATION OF LARGE-SCALE NEURONAL DYNAMICS USING ELECTROMAGNETIC FLUX

Year: 2023-2025

**In partial fulfillment of the requirement of the award of Master of
Science Degree in Physics**

By

BLESSY JOVANO | AM23PHY004

M Sc PHYSICS

Under the supervision of

Dr. Mary Vinaya

Department of PHYSICS

St. Teresa's College, Ernakulam

(Autonomous)



Department of Physics

**ST. TERESAS COLLEGE
ERNAKULAM**

(Autonomous)

(Re-accredited by the NAAC at A++ level and College with Potential for
Excellence by UGC)

MAHATMA GANDHI UNIVERSITY

MAHATMA GANDHI UNIVERSITY
PROJECT REPORT

MODULATION OF LARGE-SCALE NEURONAL DYNAMICS USING ELECTROMAGNETIC FLUX

Year: 2023-2025

**In partial fulfillment of the requirement of the award of Master of
Science Degree in Physics**

By

BLESSY JOVANO | AM23PHY004

M Sc PHYSICS

Under the supervision of

Dr. Mary Vinaya

Department of PHYSICS

St. Teresa's College, Ernakulam

(Autonomous)



Department of Physics

**ST. TERESAS COLLEGE
ERNAKULAM**

(Autonomous)

(Re-accredited by the NAAC at A++ level and College with Potential for
Excellence by UGC)

MAHATMA GANDHI UNIVERSITY


DEPARTMENT OF PHYSICS
ST. TERESAS COLLEGE (AUTONOMOUS), ERNAKULAM

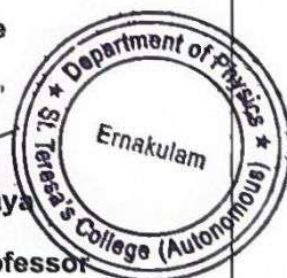


CERTIFICATE

This is to certify that the project "**Modulation of large-scale neuronal dynamics using electromagnetic flux**" is done by **Blessy Jovano** (Reg No: AM23PHY004) in partial fulfillment of the requirements for the award of the degree of Master of Science in Physics of St. Teresas College (Autonomous), Ernakulam, affiliated to Mahatma Gandhi University Kottayam during the academic year 2023-2025 under my supervision and guidance.

Project Guide


Dr. Mary Vinaya
Assistant Professor
St. Teresas College
Ernakulam



Date: 02-05-2025

Place: Ernakulam

DEPARTMENT OF PHYSICS
ST. TERESAS COLLEGE (AUTONOMOUS), ERNAKULAM



MSC PHYSICS
PROJECT REPORT

Name: Blessy Jovano | AM23PHY004

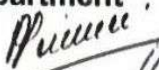
Year of work: 2023-2025

This is to certify that the project "**Modulation of large-scale neuronal dynamics using electromagnetic flux**" is done by **Blessy Jovano** (Reg No: AM23PHY004) in partial fulfillment of the requirements for the award of the degree of Master of Science in Physics of St. Teresas College (Autonomous), Ernakulam, affiliated to Mahatma Gandhi University, Kottayam and has not been included in any other MSc project submitted previously for the award of any degree.

Project Guide


Dr. Mary Vinaya

Head of the department

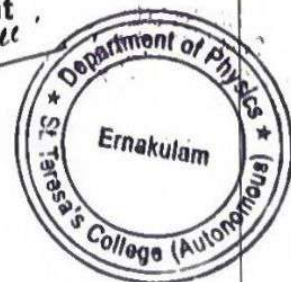

Dr. Mary Vinaya

External Examiners 1)

2)

Date: 03-05-2025

Place: Ernakulam



DECLARATION

I, **Blessy Jovano**, hereby declare that the project report entitled "**Modulation of large-scale neuronal dynamics using electromagnetic flux**" is a Bonafide record of the work carried out by me during the academic year 2023-2025 under the guidance of **Dr. Mary Vinaya**, Assistant Professor, Department of PHYSICS, St. Teresas College, Ernakulam. The data and conclusions drawn are based on the work done by me. This is my original work, and the report submitted has not been duplicated from any other source.



Blessy Jovano | AM23PHY004
St. Teresas College
Ernakulam

Date: 02-05-2025

Place: Ernakulam

AKNOWLEDGEMENT

First and foremost, I extend my heartfelt gratitude to the Almighty God for being able to successfully complete this project.

I take this opportunity to express my immense gratitude and profound admiration to my guide **Dr. Mary Vinaya**, Assistant professor and Head of the department of Physics, St. Teresas college, Ernakulam, for her exceptional direction, monitoring, support and endless inspiration without which this project would not be able to exist in the established outline.

I am extremely thankful to all other faculties of the department of physics, for their constant support.

I would like to express my gratitude to all respondents and colleagues in developing the project. I am grateful to my parents for their blessings and constant encouragement throughout the project.

**Blessy Jovano | AM23PHY004
St. Teresas College
Ernakulam**

Date:

Place: Ernakulam



ST.TERESA'S COLLEGE (AUTONOMOUS) ERNAKULAM

Certificate of Plagiarism Check for Dissertation

Author Name BLESSY JOVANO , MEGHANA VIMAL M

Course of Study M.Sc. Physics

Name of Guide Dr. Mary Vinaya

Department Physics & Centre For Research

Acceptable Maximum Limit 20

Submitted By library@teresas.ac.in

Paper Title MODULATION OF LARGE-SCALE NEURONAL DYNAMICS USING ELECTROMAGNETIC FLUX


Similarity 14% AI - 12%


Paper ID 3553691


Total Pages 46

Submission Date 2025-04-28 15:00:11


Signature of Student


Signature of Guide




Checked By
College Librarian



ABSTRACT

Electromagnetic fields have been reported to affect neuronal dynamics, although the large-scale mechanisms involved are not yet clearly understood. Here, the intention is to examine the influence of electromagnetic fields on large-scale activity in the brain through nonlinear analysis and adjustment to computational models of cortical function.

Through the insertion of novel mechanisms into proven models, simulate and compare the variations in neural oscillations, network synchrony, and distributed cognitive processes. The knowledge obtained from this research is likely to promote knowledge of brain dynamics under electromagnetic control and assist in the establishment of neuromodulation methods, brain-computer interfaces, and neurological disorder treatments linked to electrical disturbances.

CONTENTS

CHAPTER.1	09
INTRODUCTION	10
RESTING POTENTIAL	10
EQUIVALENT CIRCUITS	11
FIRING RATE	13
WILSON-COWAN EQUATIONS	16
NETWORK SYSTEM OF TWO NEURONS	17
GENERALIZED FIRING RATE MODELS	26
CHAPTER.2	28
INTRODUCTION	29
GENERAL SCHEME OF THE MODEL	29
RESULTS	32
CHAPTER.3	37
INTRODUCTION	38
MEMRISTOR	39
MEMRISTIVE NEURONS	44
MEMRISTIVE WILSON COWAN MODEL	45
MODIFIED RESULTS	45
CONCLUSION	48
REFERENCES	49

CHAPTER.1

NEURONAL DYNAMICS

INTRODUCTION

Neuroscience deals with the nervous system's structure, working, development, and degeneration in health and disease. It mainly focuses on the system of nervous. where neurons are the introductory signaling units. Neurons, similar to all cells, contain organelles to stay alive and communicate via synapses. The presynaptic neuron is to send signals, and the postsynaptic neuron is to receive signals. Presynaptic neurons release neurotransmitters, which are chemical couriers that diffuse across the synaptic cleft, the small gap between two neurons, and bind to specific receptors on the postsynaptic cell. This alters the membrane eventuality of the postsynaptic neuron, impacting its electrical state. Depending on the type of neurotransmitter released, this effect can either increase (excitatory) or drop (inhibitory) the liability of the postsynaptic neuron firing an action eventuality. Depolarization, which reduces the difference in charge across the neuron's membrane, excites the synapse and makes the neuron more likely to transmit a signal. In discrepancy, hyperpolarization increases the charge difference, making it more delicate for the neuron to reach the threshold demanded for activation, thereby inhibiting signal transmission.[10]

THE RESTING POTENTIAL

In all living cells there is an electrical voltage, or potential difference, between their inside and outside.[10] In mathematical terms, the membrane potential V_M is defined as

$$V_M = V_{in} - V_{out} \quad (1.1)$$

Where, V_{in} is the potential on the inside of the cell and V_{out} is the potential on the outside of the cell.[10] The voltage difference across a cell membrane when the cell is at rest is known as the resting potential.

An inward current corresponds to a positively charged ion, such as Na^+ , entering the cell. This raises the membrane potential; that is, it brings the membrane potential closer to zero (Depolarized). An outward current corresponds to a positively charged ion, such as K^+ , leaving the cell or a negatively charged ion, such as Cl^- , entering the cell (Hyperpolarized). The principal ions found on either side of the cell membranes are Na^+ , K^+ , and Cl^- .[10]

If the cell is permeable only to K^+ , its concentration gradient drives K^+ ions out, leaving behind a negative charge inside. This buildup of charge gradually opposes further K^+ discharge until an equilibrium is reached, where electrical and chemical forces are balanced. The membrane potential at this equilibrium is known as the K^+ Nernst equilibrium or reversal potential.[10]

$$E_k = \frac{RT (\ln[K^+]_{out}/[K^+]_{in})}{zF} \quad (1.2)$$

Where, z is the valence of the ion ($\pm 1, \pm 2$, etc.) and F is the Faraday constant. In general, we can write above *Nernst equation* as,

$$V_{eq} = V_{in} - V_{out} = - \frac{RT (\ln[C]_{out}/[C]_{in})}{zF} \quad (1.2A)$$

Goldman-Hodgkin-Katz equation is an equation which gives an explicit expression for how the resting potential depends on the concentrations, both inside and outside, of ions and the permeabilities of the membrane to the ions.[10]

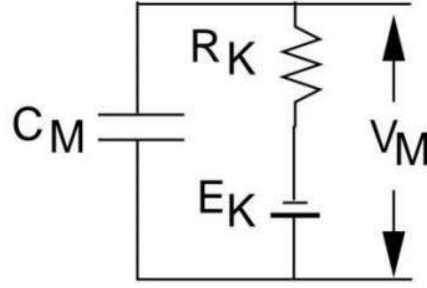
$$V_M = \frac{RT}{F} \ln \frac{P_K[K^+]_{out} + P_{Na}[Na^+]_{out} + P_{Cl}[Cl^-]_{in}}{P_K[K^+]_{in} + P_{Na}[Na^+]_{in} + P_{Cl}[Cl^-]_{out}} \quad (1.3)$$

The dissipation of ionic gradients is prevented by active pumps that extrude Na^+ ions from the cell while taking in K^+ . The Na^+ - K^+ pump is an integral membrane protein that exchanges three Na^+ ions for two K^+ ions. [10]

EQUIVALENT CIRCUITS

A very helpful means to describe the reaction of the membrane potential is through the language of electrical circuits; it is usually referred to as the equivalent circuit model. The circuit includes three elements: (1) resistors or conductors, which are the ion channels; (2) batteries, which are the concentration gradients of the ions; and (3) capacitors, which are the membrane's capability to hold charge. The equivalent circuit model [10] results in deep understanding of how ion movement creates electrical signals in the nerve cell. capacitors have charge which they release subsequently in the form of currents. If C_M is membrane capacitance, the charge stored and potential relationship is:

$$q = C_M V_M \quad (1.4)$$



The specific membrane capacitance(C_M) is known as capacitance per square centimeter. Since current is the time derivative of charge, we can differentiate above expression for the specific capacitance current equation:[10]

$$I_{cap} = C_M \left(\frac{dV_M}{dt} \right) \quad (1.5)$$

If \hat{g}_K is the conductance of a single K^+ channel, then,by using Ohm's law, the ionic current through this channel is

$$\hat{I}_K = \hat{g}_K(V_M - E_K) \quad (1.6)$$

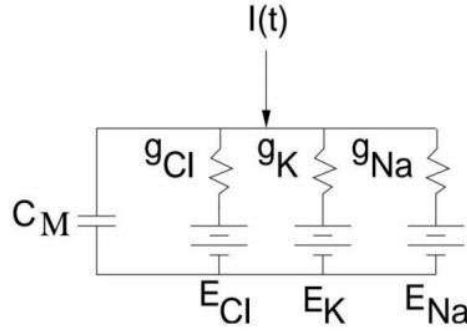
If there is N_K potassium channels in a unit area of membrane, the conductance per unit area, or specific membrane conductance (S/cm^2) is given by $g_K = N_K \times \hat{g}_K$ and specific membrane resistance ($\Omega \cdot cm^2$) is $r_K = \frac{1}{g_K}$ [10] Then,

$$I_K = \frac{(V_M - E_K)}{r_K} \quad (1.7)$$

By Kirchhoff's current law,

$$0 = I_{cap} + I_K = C_M \left(\frac{dV_M}{dt} \right) + \frac{(V_M - E_K)}{r_K} \quad (1.8)$$

Figure below shows an equivalent circuit with three parallel conductance and a current source, $I(t)$. [10]



The ionic current, per unit area, is given by

$$i_{\text{ion}} = g_{\text{Cl}}(V_M - E_{\text{Cl}}) - g_{\text{K}}(V_M - E_{\text{K}}) - g_{\text{Na}}(V_M - E_{\text{Na}}) \quad (1.9)$$

Thus, we can write

$$C_M \left(\frac{dV_M}{dt} \right) = \frac{-(V_M - r_M)}{r_M} + \frac{I(t)}{A} \quad (1.10)$$

where,

$$E_R = g_{\text{Cl}}E_{\text{Cl}} + g_{\text{K}}E_{\text{K}} + g_{\text{Na}}E_{\text{Na}} \quad (1.11)$$

is the cell's *resting potential* and

$$r_M = \frac{1}{(g_{\text{Cl}} + g_{\text{K}} + g_{\text{Na}})} \quad (1.12)$$

is the *specific membrane resistance*.

Permeability is a function of the state of the membrane, whereas conductance is a function of ion concentration as well. K^+ permeability can be high with numerous open channels, yet conductance will be low if K^+ concentration is low on both sides of the membrane. [10]

FIRING RATE

Firing rate is used to describe how many action potentials a neuron gives off over some duration of time. It is a key value in the area of neuroscience as it allows us to know that neurons encode information and send out information. The rate coding hypothesis postulates that brain information is not encoded in the precise timing of individual spikes but in firing frequency variation. A high firing rate would correspond

to a high-strength stimulus, and a lower one might correspond to a lower or less salient stimulus. This is the tacit assumption of much of the work of current neuroscience, e.g., studies concerning how the brain comes to experience, understand, and react to its world. [3,4]

Firing Rate and cognitive functions

Brain firing rates are not constant; they change dynamically and comparatively quickly in reaction to varying stimuli. This flexibility enables neurons to keep pace with arriving sensory input, thus enabling the brain to interpret and react to that information in real-time. These variations in firing rate can take place within just 10 milliseconds, and that is needed in order to rapidly react to changing circumstances in the world. For instance, if a person is subjected to a flash of light or a sudden noise, the neurons within the visual or the auditory cortex can abruptly accelerate the firing rate to deliver quick awareness and reaction. The capacity of neurons to alter their firing rate is vital for a wide range of cognitive processes. For perception tasks, the neurons of the sensory cortex modulate their firing rate to accommodate the nature of the stimulus, i.e., intensity or direction. For decision tasks, some populations of neurons will enhance their firing rate as the brain accumulates evidence for one option over another. Motor control is also regulated by firing rates in controlling muscle contraction strength and timing. These operations are not local but take place on networks of cooperating neurons, which shows the distributed nature of brain operation. [4,5]

Relationship between Firing Rate and Membrane Potential

Of the most influential factors in shaping a neuron's firing rate, one is the membrane potential the difference in electric charge between inside and outside a cell. The resting membrane potential of a neuron is approximately 70 millivolts. When there is input from other cells that makes the membrane potentially less negative, the cell is nearing a threshold, typically near 55 millivolts. When the threshold is reached, the neuron emits an action potential. The more times the threshold is reached, the greater the firing rate of the neuron. By comparison, inhibitory inputs hyperpolarize the neuron, moving the membrane potential away from the threshold and decreasing the rate of firing. The relationship between membrane potential and the rate of firing is nonlinear. As the membrane potential of a neuron gets close to the threshold, small changes can significantly increase the rate of firing. This renders neurons very sensitive to input close to their threshold. There are neurons that will continue to fire at regular periods with input and others with more complicated behavior, like burst firing or rhythm oscillations. These are dependent on the type of ion channels and receptors possessed by the neuron and its place in the nervous system in terms of function and structure. [3,6]

Estimating Firing Rates from Neural Data

Estimating and quantifying firing rates from experimental observations is challenging because of variability in spike timing. The neurons never fire at a uniform rate even if the same stimulus is presented to them several times, their response may differ. To interpret this variability, researchers apply several techniques that examine spike trains, which are series of when a neuron fires. One of the most common is the peri-stimulus time histogram (PSTH), which sums spike activity over a large number of trials to get a better picture of the relationship between firing rate and time. Another is kernel smoothing, in which mathematical processes are used on spike data to produce a smooth estimate of firing rate. More advanced techniques, such as spike train analysis, use statistical models to fit spike patterns and infer conclusions regarding underlying neural processes. These estimation protocols are the focal point of experimental neuroscience and computational models. They are capable of measuring how the neurons react to stimulus, talk with one another, and how information travels through the brain. Firing rates have also been instrumental in the creation of brain-computer interfaces, where recorded neural signals are converted into commands for controlling external devices. For these applications, minor variations in firing rate could be used to control a cursor on the computer screen, index a robot arm, or even restore the function of paralyzed limbs. [6,5]

Relevance in Neural Modeling and Brain-Computer Interfaces

The idea of firing rate reduces the complexity of neural activity to a more manageable form, which is easier to analyze and model, particularly when trying to model populations of hundreds or thousands of neurons. Although the brain can encode information in more nuanced ways e.g., by spike timing or synchrony firing rate is still a convenient and handy measure for the analysis of neural coding. Furthermore, its connection to the membrane potential closes the gap between the biophysical operations of single neurons and the emergent computations of neural networks. [5,3]

FIRING RATE MODEL

Firing rate model is one of the most general methods for simulating big neural networks. These models consider the mean firing activity of populations of neurons in a network, rather than modeling the actual spiking behavior of each neuron. Sometimes they are called population models, but they represent the ensemble dynamics of assemblies of neurons and not cells. Here, it is also known as rate models, although the variable is supposed to represent may not certainly always be identical with a neuron's firing rate. In general, there is an invertible mapping between the model variable and the actual firing rate. The equations for rate models are derived in different kinds some through strict biophysical derivations, some by more heuristic

or ad hoc methods. Once developed, these models are used in a broad variety of intriguing phenomena, from working memory to hallucinations, binocular rivalry to optical illusions, and traveling waves. While much of this work is based on a general review by one of the authors (GBE), we also include recent analysis from the Omurtag, Knight, and Cai studies.[10] Firing rate models are popular for a number of good reasons. Foremost among them is computational parsimony simulating large.[10]

Networks of conductance-based neurons can overwhelm even the most sophisticated computers. Consequently, a number of large-scale simulations resort to easier spiking models such as the integrate and fire model, or resort to rate models for ease of tractability. Additionally, most experimental methods do not record a neuron's internal voltage directly but instead record its probability of firing. Extracellular recordings, for example, record spikes without reporting subthreshold activity. In these cases, modeling firing rate is more appropriate than membrane potential modeling. Methods such as field potential recordings, EEG, and fMRI report the activity of large groups of neurons and thus population-level models are not only appropriate but, in many cases necessary to make sense of the data. In fact, rate models are some of the earliest and longest-lasting forms of brain modeling and their simplicity, speed, and connection to experimental evidence remain reasons they are such important tools in neuroscience.[10]

THE WILSON COWAN EQUATIONS

One of the most influential models in the neural network literature is the one developed by Hugh Wilson and Jack Cowan.[10] The original equations have the following form:

$$\tau_e \frac{dE}{dt} = -E + (1 - r_e E) F_e(\alpha_{ee} E - \alpha_{ie} I + T_e(t)) \quad (1.13)$$

$$\tau_i \frac{dI}{dt} = -I + (1 - r_i I) F_i(\alpha_{ei} E - \alpha_{ii} I + T_i(t)) \quad (1.14)$$

where T_j is the input from the thalamus and r_e, r_i represent the refractory fraction of the neurons available to fire. The term $(1 - r_e E)$ is an approximation of

$$1 - \int_{t-r_e}^t E(s) ds \quad (1.15)$$

which represents the fraction of neurons available to fire given that they have an absolute refractory period of r_e . In a recent paper, Curtu and Ermentrout analysed the behaviour of the original integro - differential equations for a single excitatory population. The extra pro-multiplicative factor $(1 - r_e E)$ does not make too much of a difference in the analysis of the equations so we will generally set $r_e = r_i = 0$. We first consider a single scalar model for one recurrent population of neurons. Then we turn

to the pair and we will look at mutually excitatory, inhibitory, and mixed populations. The last case is the WC equations.[10]

A note on the gain functions: The traditional form for this is the logistic function, $F(u) = 1 / (1 + \exp(-\beta(u - u_T)))$, which we have also encountered in our study of voltage-gated conductance. With the use of a logistic function, we interpret the function F as a probability of firing rather than an actual firing rate. Another similar choice for F is $F(u) = 1 + \text{erf}(u)$ where $\text{erf}(u)$ is the error function (integral of a Gaussian). Pinto et al. use this model to study the mean field approximation for a model of cortex.[10] If we regard F as an actual firing rate of a single cell, then we could use an approximation for a neuron which undergoes a saddle-node bifurcation to periodic firing; namely:

$$F(u) = A \sqrt{\max(u - u_T, 0)} \quad (1.16)$$

where u_T is the minimal current needed to induce firing. This gain function is continuous, but not differentiable and so will lead to problems when it comes time to numerically analyse models.[10]

$$F(u) = A \sqrt{(u - u_T) / (1 - \exp(-\frac{u - u_T}{\beta}))} \quad (1.17)$$

$$F(u) = A \sqrt{\beta \log[1 + \exp(\frac{u - u_T}{\beta})]} \quad (1.18)$$

Here, β is a measure of the "noise"; as $\beta \rightarrow 0$, both these functions approach a pure Square - root model. There are two more functions which are commonly encountered:

(i) the step function for which the neuron either is not firing at all or is firing at the maximal rate. This turns out to be the easiest to analyse and we will return to it when we get to networks.[10]

(ii) the piecewise linear function $F(u) = \max(u - u_T, 0)$. Linearity makes it possible to also analyse this function. Aside from the fact that it can be analysed, there is not much to say in favour of the piece-wise linear function. Our strongest criticism of the piecewise linear function is that the firing rate can go to infinity in recurrent networks. The step function and the logistic function, which both saturate, do not have this trouble. The square-root model is sublinear for large inputs so that it also does not "run away." [10]

NETWORK SYSTEM OF TWO NEURONS

The systems whose interactions among the cells are identical, either excitatory or inhibitory. The next theorem makes it possible to concentrate on fixed points only:

Theorem.

Let the planar system:

$$x' = f(x, y) \quad (1.19)$$

$$y' = g(x, y) \quad (1.20)$$

be such that $f_y g_x > 0$ for all (x, y) . Then there are no limit cycles.[10]

From this it is noted that this bears a resemblance to Bendixson's negative criterion, which states that if $f_x + g_y$ is of fixed sign in a region R, then there will be no limit cycles contained wholly in R. An obvious consequence of this is that for the two-population neural model:

$$T_1 u_1' = -u_1 + F_1(w_{11}u_1 + w_{12}u_2) \quad (1.21)$$

$$T_2 u_2' = -u_2 + F_2(w_{21}u_1 + w_{22}u_2) \quad (1.22)$$

If $F_j'(u) > 0$ and $w_{12}w_{21} > 0$, then no fixed points can be present, i.e., limit cycles do not exist, only fixed points can. So, the whole phase portrait can be studied by going through the intersection of the nullclines.[10]

It is supposed that F_j are saturating nonlinearities with maximum value 1 and minimum value 0, without loss of generality. They are also supposed to be monotonically increasing with a single inflection point. Let G_j be the inverse of F_j . $G_j(x)$ have vertical asymptotes at $x=0$ and $x=1$ and are monotonically increasing.[10]

The u_1 nullcline is given by:

$$u_2 = (G_1(u_1) - w_{11}u_1)/w_{12} \equiv H_1(u_1) \quad (1.23)$$

If, $w_{11} < 0$, then H_1 is a monotonically similar function to G_1 . But if, $w_{11} > 0$, and the self-link is strong enough, then H_1 can form a cubic-like shape. Same goes for the nullcline; if $w_{22} > 0$, it can form a "cubic" too.

Fig. 1.1A and 1.1B depict a number of possibilities. The u_1 nullcline can be displaced vertically by adjusting the inputs, but the u_2 nullcline can be displaced horizontally. Depending on the arrangement, the system can have as few as one or as many as nine fixed points. Bifurcations are generally saddle-node types, although a symmetric case resulting in a pitchfork bifurcation is later described.[10]

If both nullclines are "cubic," the outer and middle branches of the cubic can be determined. Any fixed point at the intersection of two outer branches is a stable node,

while those on the inner branches are unstable nodes. The rest are saddle points. This is left as an exercise to the reader who is interested. Saddle points are important, since their stable manifolds are separatrices that separate the plane into regions of attraction for the several stable fixed points. Fig. 1.1C illustrates an example: a mutually excitatory network with two stable states one in which both populations fire at a low rate and another at a high rate.[10]

Prior to studying excitatory-inhibitory networks, which have the richest dynamics, a key and frequent example is discussed. Most cognitive and other functions involve the selection of two or more incompatible sensory inputs. For example, picture carrying a reliable musket: on your left, an oncoming lion, and on your right, an oncoming pug. Where to look is quite evident. But if one is substituted with another pug, most probably the reaction is to disregard both except in the case of a specific reason, like preference for or aversion to dogs. When two lions' approach, however, there is a tendency to select one haphazardly, particularly where one seems nearer, incorporating a bias. Fig.1.2A introduces a competition model between two pools of neurons, pool 1 and pool 2. They both get an input and inhibit each other. As this illustration shows most of the math of the concepts mentioned in the course of this chapter, the details are mainly drawn out. Inputs are described as: $I_1 = I (1+ a)$ and $I_2 = I (1-a)$ where a is an asymmetry parameter and I is the total input.[10]

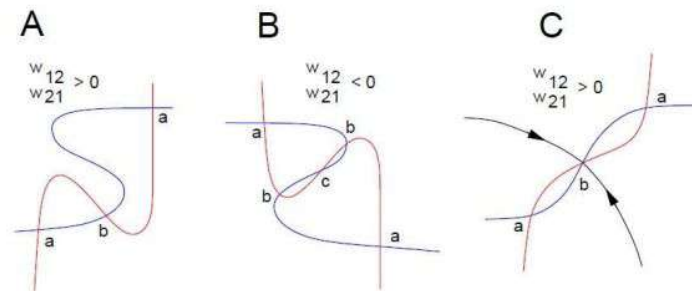


Fig. 1.1 Nullcline configurations for mutually excitatory/inhibitory networks (A) mutual excitation, (B) mutual inhibition, (C) mutual excitation with weak self-connections.[10]

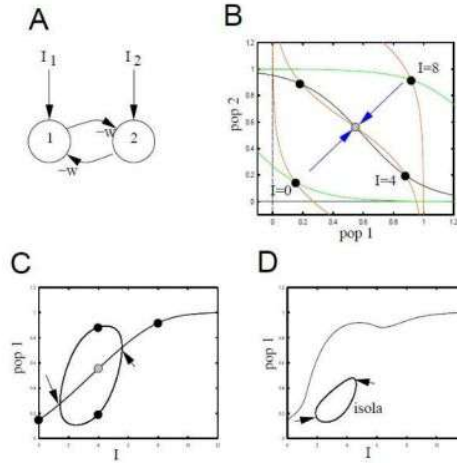


Fig. 1.2 The simplest model for competition between two populations. (A) the circuit (B) nullclines for identical inputs at 3 different strengths (C) bifurcation diagram when the inputs are identical (D) same as (C) but there is a small bias to population 1[10]

When $a=0$, the input is unbiased and does not favor either unit. The extreme asymmetry case would have $a=\pm 1$. The analysis will be limited to the case $a=0$ and leave the $a\neq 0$ case for numerical study. The equations to be considered are:

$$u_1' = -u_1 + F(I - wu_2) \quad (1.24)$$

$$u_2' = -u_2 + F(I - wu_1) \quad (1.25)$$

Suppose that F is a monotone increasing, positive function with $F'(x) \rightarrow 0$ as $x \rightarrow \infty$ and that F is bounded. The weight $w \geq 0$. Because of the symmetry of the system, one solution is the homogeneous state, $u_1 = u_2 = \bar{u}$ and

$$\bar{u} = F(I - w\bar{u}) \quad (1.26)$$

Leave it as an exercise to demonstrate that this homogeneous equilibrium point is unique, positive, and is a monotonically increasing function of I and decreasing function of w . Let $c = F'(I - w\bar{u}) > 0$, the derivative of F at the equilibrium. The Linearizing equation (1.24 & 1.25) is:

$$v_1' = -v_1 - cwv_2 \quad (1.27)$$

$$v_2' = -v_2 - cwv_1 \quad (1.28)$$

This is a simple 2×2 matrix, A . Instead of directly calculating the eigenvalues, the focus now shifts to matrices with a special form, called circulant matrices.

Let a_0, \dots, a_{n-1} be fixed numbers (real or complex) and consider the matrix, A formed as follows:

$$A = \begin{pmatrix} a_0 & a_1 & \dots & a_{n-1} \\ a_{n-1} & a_0 & \dots & a_{n-2} \\ \vdots & \vdots & \ddots & \vdots \\ a_1 & a_1 & \dots & a_0 \end{pmatrix}.$$

Such a matrix is called a circulant matrix and the eigenvectors and eigenvalues are easy to write down. Let $z_k = \exp(2\pi i k/n)$ for $k = 0, \dots, n-1$. Let \vec{v}_k be the column vector whose j^{th} entry is z_k^{j-1} . Then \vec{v}_k is an eigenvector for A and the eigenvalue is

$$\lambda_k = \sum_{j=0}^{n-1} a_j z_k^j.$$

For example, if $n = 2$, then the eigenvectors are $(1, 1)^T$ and $(1, -1)^T$ with eigenvalues $a_0 + a_1$ and $a_0 - a_1$ respectively.

Since the linearization, A is a circulant matrix, the eigenvectors and eigenvalues are $\{(1, 1), -1 - cw\}$ and $\{(1, -1), -1 + cw\}$. The first of these eigenvalues is always negative; thus, any homogeneous perturbation (along the eigenvector, $(1, 1)$) decay to zero. If w is large enough, then $-1+cw$ will be positive across some range of inputs I , so asymmetric perturbations along the direction $(1, -1)$ can grow over time. At some critical input value I_0 , the associated eigenvalue crosses zero, marking the beginning of a bifurcation. Because of the symmetry inherent in the system, this is not a standard fold bifurcation but a pitchfork bifurcation, one that is often found in systems described by circulant matrices. As the instability grows along the asymmetric eigenvector, the resulting bifurcated solutions will mirror its structure.[10]

$$(u_1, u_2) = (\bar{u} + r, \bar{u} - r) \quad (1.29)$$

The solution's amplitude is represented by $|r|$, with r either positive or negative determining whether u_1 or u_2 "wins." Fig.1.2B shows the phase plane and

nullclines of equation (1.24&1.25), with, $F(u) = \frac{1}{1+\exp(-(u-1))}$, $w=5$ and I as a variable parameter.[10]

Both units fire equally at low input values, arriving at the same steady state. For intermediate levels of input, this symmetric fixed point loses stability and produces two stable fixed points, each corresponding to dominance by one unit. A saddle point (represented by a grey circle) has a stable manifold (blue arrows) that separates the phase plane into two regions: trajectories in the upper left approach the u_2 -dominant state, and those in the lower right approach the u_1 -dominant state. Therefore, without input bias, the ultimate fate hinges on the two units' initial conditions.[10]

Under high inputs, symmetry is re-established, and both units fire strongly at high rates, resulting again in a single homogeneous solution. Fig. 1.2C shows the bifurcation diagram for the symmetric input situation: between two arrows, one or the other unit prevails.[10]

When a slight bias is applied, the preferred unit always emerges victorious as input increases (Fig. 1.2D). Yet, if the perturbation is strong enough, it may shift dominance transiently to the less preferred unit over a range of limited input. This dynamic creates an Isola a bounded loop or separated branch of solutions between a pair of fold bifurcations (marked by arrows). As the bias reduces, the Isola increases in size and, at a large enough bias, recombines with the primary solution branch to restore the symmetric bifurcation structure of Fig. 1.2C. By contrast, as the bias increases, the Isola decreases in size to a point and vanishes.[10]

This example summarizes symmetry-breaking instabilities and bifurcations: a symmetric solution loses stability because of competitive interactions to give rise to asymmetric patterns and novel, more sophisticated behavior.[10]

Excitatory-inhibitory pairs.

Focus on two population models in which one population is excitatory and the other inhibitory:

$$\tau_1 u_1' = -u_1 + F(w_{11}u_1 - w_{12}u_2 + I_1) \quad (1.30)$$

$$\tau_2 u_2' = -u_2 + F(w_{21}u_1 - w_{22}u_2 + I_2) \quad (1.31)$$

$u_1(u_2)$ is the excitatory (inhibitory) population. It is possible to do a sufficiently detailed local bifurcation analysis of this system if the inputs are the main

parameters. Borisjuk and Kirillov provide such an analysis when $F(u) = \frac{1}{1 + \exp(-(u-1))}$; Hoppensteadt and Izhikevich perform a similar analysis.[10] Choosing this F has the advantage of allowing us to note that

$$\frac{dF}{du} = F(1-F) \quad (1.32)$$

Let,

$$G(y) = \ln \frac{y}{1-y} \quad (1.33)$$

be the inverse of $F(u)$. At an equilibrium point, we can solve for I_j :

$$I_j = G(u_j) - w_{j1}u_1 + w_{j2}u_2 \quad (1.34)$$

Let $B_j = w_{j1}u_1 - w_{j2}u_2 + I_j$ be the total input into each population. The linearization matrix has the form:

$$A = \begin{pmatrix} -1 + w_{11}F'(B_1) & -w_{21}F'(B_1) \\ w_{12}F'(B_2)/\tau & (-1 - w_{22}F'(B_2))/\tau \end{pmatrix}$$

The formula $F'(B_j) = u_j(1 - u_j)$ can be obtained by applying the equilibrium condition $F(B_j) = u_j$ and the identity $F' = F(1 - F)$. Two types of bifurcations are present in this model: Hopf and saddle-node bifurcations. Saddle-node bifurcations can be understood by considering where the nullclines cross. For the Wilson-Cowan (WC) network, there can be as many as five different fixed points. Hopf bifurcations can be determined directly with the above identities. A sufficient condition for the existence of imaginary eigenvalues in the matrix A is that its trace vanishes.[10]

$$\text{Tr} \equiv -1 + w_{11}u_1(1 - u_1) - 1/\tau - w_{22}u_2(1 - u_2)/\tau = 0. \quad (1.35)$$

To explain, unless $w_{11} > 4$, the trace is always going to be negative as $0 < u_j$ and $u_j < 1$. This implies that we require ample recurrent excitation. Now that $u_1 = u_1^\pm(u_2)$, we are left with a quadratic equation, thus we can solve it to achieve two roots. We can then write I_1 and I_2 as functions of the single parameter u_2 by substituting $u_1 = f(u_2)$ back into equations (1.34). To determine the curves of the Hopf bifurcation points, we vary u_2 between 0 and 1 for each branch of $u_1^\pm(u_2)$. The determinant in this case is quartic in u_1 and u_2 and hence more difficult to deal with in closed form. Therefore, this method is not practical for finding the fold curve when the determinant is zero.[10]

The best method for calculating such diagrams is by numerical means. Fig. 1.3 shows the dynamics of this network with a set of fixed weights and a constant time parameter. As the excitatory input is increased, the resting state increases until it becomes unstable at a Hopf bifurcation. Because increasing I_1 raises the u_1 nullcline up, this effect is evident in Fig. 1.3C. On low levels of input, the excitatory nullcline cuts the inhibitory nullcline along a branch of negative slope, suggesting a stable fixed point. When the input increases, the point of intersection moves to the middle branch, where it will eventually become unstable and lead to a Hopf bifurcation and the appearance of a limit cycle. Interestingly, while the input is further raised, the excitatory nullcline gets closer to the top portion of the inhibitory nullcline, causing an increase in the period of the limit cycle. With input levels very high, the nullclines intersect at higher values of excitation and inhibition.[10]

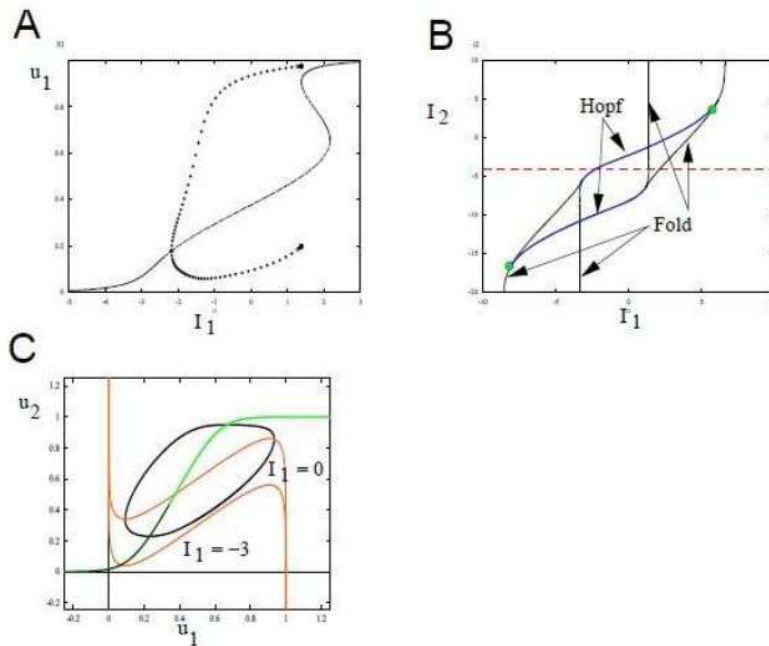


Fig. 1.3 Sample bifurcation diagram for an excitatory and inhibitory population. Parameters are $w_{11} = 12$, $w_{12} = 10$, $w_{21} = 16$, $w_{22} = 4$, $\tau = 2$. (A) Behaviour of u_1 as I_1 increases, $I_2 = -4$. (B) Two parameter diagrams as a function of the inputs, I_1 , I_2 . Green circle indicates Takens-Bogdanov points. (C) Phase plane for $I_2 = -4$, $I_1 = 0$.

Up-down states: Recent experiments on prefrontal cortical slices have shown that local networks of excitatory and inhibitory neurons can generate epochs of sustained firing both spontaneously and in response to external stimuli. These two clearly differentiated states firing (active) and resting are apparent on both extracellular and intracellular recordings. An example of the latter type of

recording is given in Fig. 1.4A of a cortical slice preparation that preserves the excitatory and inhibitory circuitry. The network exhibits repeated periods of sustained activity that may extend for as long as four seconds, interrupted by epochs of silence. Intracellular recording from one of the pyramidal neurons in the network illustrates that during active periods, the membrane potential is heavily depolarized the "up state" relative to the hyperpolarized "down state" during silent periods. Transitions among such states can be triggered by external stimulation, with depolarizing inputs capable of toggling the network from the down to the up state and the up to the down state. Contrary to expectation, sufficiently powerful depolarizing stimuli can actually cause a transient burst of activity even when the network is in its down state, though this normally results in an immediate return to quiescence.[10]

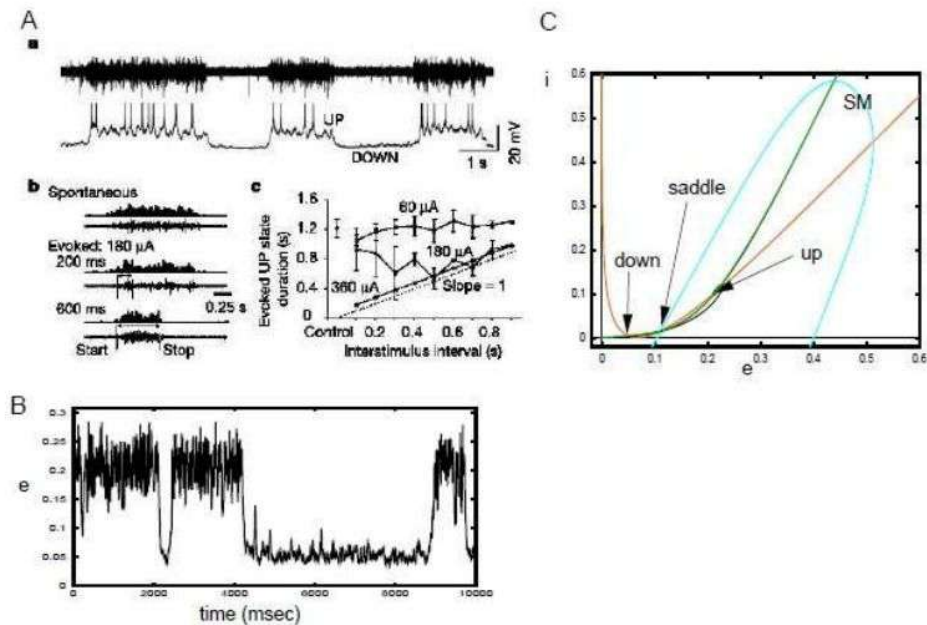


Fig. 1.4

Fig. 1.4B shows a simulation of equations (1.30,1.31) when there is coloured noise added to the inputs. The noise is needed to effect spontaneous switching between states.

A simple explanation of up and down state properties can be proposed on the basis of equilibrium between inhibition and excitation.

Fig. 1.4C is the silent phase plane of panel B's simulation. As anticipated, the system has two stable fixed points for the down and up states of the network, with a saddle point separating them whose stable manifold acts as a dynamic threshold between them. In bistable systems like the one in Fig. 1.2B, the topography of the stable manifold usually means that only negative perturbations

can push the system from the up to the down state. But with the curved stable manifold of the up-down model, strong depolarizing inputs also cause transitions from the up to the down state. As one can observe from Fig. 1.4C, the down-manifold of the saddle point wraps around such that if a stimulus drives the excitatory population above approximately 0.4, the system returns to down state immediately. But intermediate stimuli can flip the system from up to down state or from down to up state. This model explains many of the characteristics of up and down states which have been observed. As a particular example, an upstate depolarizing shock will cause a transition to the down state. Transitions between states will exhibit a stimulus-dependent delay. As the figure makes evident, stimuli close to the right-hand branch of the stable manifold take longer to cause a state transition than bigger stimuli, which switch more quickly. Also, intense stimuli in the down state can initiate a short burst of activity and fast return to rest. Adding a little bit of noise into the model will introduce spontaneous up-to-down and down-to-up switching, like Fig. 1.4A. Since the up state is closer to the boundary of instability and has complex eigenvalues, perhaps this is why the up state is more variable and noisier compared to the down state that is stable.[10]

Generalized firing rate models

Firing rate models can be extended with mechanisms like spike-frequency adaptation, a process that is on a much slower timescale than inhibition and one that depends completely on the activity of the individual neuron and not on network activity. Short-term synaptic plasticity, which includes mechanisms like synaptic depression and facilitation, is another important mechanism. Adaptation can be added to models as a negative feedback process based on activity. A basic population of excitatory units with adaptation can be modelled as follows:

$$\tau \frac{du}{dt} = F(u - cz) \quad (1.35)$$

$$\tau_z \frac{dz}{dt} = R(u, z) - z \quad (1.36)$$

Where, $R(u, z)$ is the activation of the adaptation mechanism through excitation. There are a number of possible formulations for this function. The simplest is to assume a linear one, $R(u, z) = u$, which already leads to a variety of interesting dynamics. But keeping in mind that F is the firing rate, a more realistic biological model would define $R(u, z) = \alpha F$ with α being a scaling constant. Furthermore, if adaptation occurs due to processes like ion channel conductance that inevitably saturate, a more suitable model would involve nonlinear saturation phenomena, which would result in a formulation of the form:

$$R(u, z) = \alpha F (1 - z) \quad (1.37)$$

This definition guarantees that adaptation is still bounded and never more than 1. It is recommended to develop this model, for instance, by analysing the case where $\tau_z \gg \tau$.

Synaptic depression (or facilitation) is more intriguing since its impact is multiplicative in the firing rate, the synaptic depression model is:

$$\frac{dd}{dt} = \frac{1-d}{\tau_d} - a_d Fd \quad (1.38)$$

If the models of the firing rate are obtained from synaptic dynamics, then F is the firing rate, but if we are estimating a noisy model neurons response to inputs, then u is the estimation of the firing rate.[10]

CHAPTER.2

Review: Feedforward and feedback frequency-dependent interactions in a large-scale laminar network of the primate cortex

INTRODUCTION

Interplay among top-down and bottom-up processing in the cerebral cortex is responsible for the decryption of attentional processes, predictive coding, executive control, and a broad assortment of other brain functions. Circuit mechanisms of these processes are generally unknown, prompting a multiscale approach that will integrate structural and dynamic features of cortical function. To answer this, a computational representation of the primate cortex was built from directed and weighted anatomical connectivity. This model includes laminar structure and replicates dynamic interactions at intralaminar, interlaminar, interareal, and whole-cortex scales.[1]

Dynamics were added to the large-scale cortical circuit by simulating each local circuit with interacting excitatory and inhibitory neuronal populations. This arrangement allows the supragranular and infragranular layers to have different oscillatory dynamics fast gamma rhythms (30–70 Hz) and slower alpha-beta rhythms (8–15 Hz), respectively. With this layered architecture, the model covers four spatial scales: intralaminar, interlaminar, interareal, and large-scale cortical levels.[1]

The model illustrates that feedforward transmission is primarily reinforcing gamma-band oscillations, whereas feedback projections have a modulatory effect mainly on alpha and low-beta frequencies. These results are consistent with current neurophysiological evidence and uncover a frequency-dependent functional hierarchy among visual cortical areas, as determined by Granger causality analysis. The model also suggests possible mechanisms through which this functional hierarchy can be dynamically reconfigured according to contextual requirements. In summary, the findings emphasize the critical functions of structural connectivity, frequency-specific communication, and feedback modulation in determining large-scale cortical dynamics. This framework provides a basic building block for future research into cognitive functions based on realistic large scale brain models.[1]

General scheme of the model

Large-scale model includes four distinct levels of description: (i) local populations that capture the activity within individual cortical layers, (ii) inter-laminar circuits that couple supragranular and infragranular layers, (iii) inter-areal couplings that reflect layer-

specific influences between cortical areas (such as V1 and V4), and (iv) a large-scale laminar cortical network that integrates anatomical connectivity data to represent 30 cortical areas distributed across the occipital, temporal, parietal, and frontal lobes.[2]

The dynamics of recurrently connected populations are described by Wilson-Cowan equations of the form:

$$\tau_E \frac{dr_E}{dt} = -r_E + \Phi(I_E^{net} + I_E^{ext}) + \sqrt{\tau_E} \xi_E(t) \quad (2.1)$$

$$\tau_I \frac{dr_I}{dt} = -r_I + \Phi(I_I^{net} + I_I^{ext}) + \sqrt{\tau_I} \xi_I(t) \quad (2.2)$$

where r_{EI} are the (dimensionless) mean firing rates of the excitatory and inhibitory populations, respectively, τ_{EI} are the corresponding time constants, ξ_{EI} are Gaussian white noise terms of strengths σ_{EI} , and $\Phi(x) \equiv x/(1+e^{-x})$ is the transduction function. The network input, $I_{E,I}^{net}$ is the input arriving to the corresponding population (the excitatory and inhibitory one, respectively) from other populations in the network (from the same layer, a different layer or different areas), and the term $I_{E,I}^{ext}$ is the input from external sources such as sensory stimuli, thalamic input, or cortical areas not explicitly included in the model.[2]

Intra-laminar local circuit

Taking into account only local contributions (i.e. assuming an isolated intra-laminar populations) the network input is given by

$$I_E^{net} = J_{EE}r_E + J_{EI}r_I \quad (2.3)$$

$$I_I^{net} = J_{IE}r_E + J_{II}r_I \quad (2.4)$$

Where $J_{\alpha\beta}$ is the mean synaptic strength from population β to population α . For the circuit in the superficial layer, parameter values are $\tau_E = 6\text{ms}$, $\tau_I = 15\text{ms}$, $J_{EE} = 1:5$, $J_{IE} = 3:5$, $J_{EI} = -3:25$, $J_{II} = -2:5$, and $\sigma_{EI} = 0:3$. For the infragranular circuit, parameters are the same except for $\tau_E = 30\text{ms}$, $\tau_I = 75\text{ms}$ and $\sigma_{EI} = 0:45$. With these parameter values the circuit displays irregular noise-driven oscillations in the gamma (supragranular) or alpha (infragranular) rhythms.[2]

Inter-laminar interactions

To couple the supragranular and infragranular layers together, Interlaminar connectivity strength is taken into account based on estimates from anatomical data and physiological studies, as in for simplicity, keep only the strongest connections in each direction between layer 2/3 and layer 5, which are the excitatory projections from

layer 2/3 pyramidal neurons to layer 5 pyramidal neurons (with strength $J_{5,2}$), and the ones from layer 5 pyramidal neurons to layer 2/3 interneurons (with strength $J_{2,5}$) as reported. The hypothesis is that these strong projections serve as an estimation of the effective connectivity between both layers, and that a certain set of core features of inter-laminar oscillatory entrainment can be explained in this framework. Following estimations for these projections, we set $J_{5,2} = 1$ and $J_{2,5} = 0.75$. Using a matrix notation for convenience, and considering only intra-laminar and inter-laminar projections, the input arriving to each one of the four populations of a given cortical area is [2]

$$\begin{bmatrix} I_{L2E} \\ I_{L2I} \\ I_{L5E} \\ I_{L5I} \end{bmatrix} = \begin{bmatrix} J_{EE} & J_{EI} & 0 & 0 \\ J_{IE} & J_{II} & J_{2,5} & 0 \\ J_{5,2} & 0 & J_{EE} & J_{EI} \\ 0 & 0 & J_{IE} & J_{II} \end{bmatrix} \times \begin{bmatrix} r_{L2E} \\ r_{L2I} \\ r_{L5E} \\ r_{L5I} \end{bmatrix}$$

Using the connectivity matrix, the input to each cortical population is given by:

$$I_{\alpha} = J_{\alpha} r_{\alpha} \quad (2.5)$$

I_{α} and r_{α} represent input and activity vectors respectively.[2]

Inter-areal interactions

The layer-specific connectivity pattern between two cortical areas (such as V1 and V4, which we will take as an example here). This pattern strongly depends on the positions of the areas relative to each other in the anatomical hierarchy for simplicity assume a pure feedforward (FF) relationship in the direction $V1 \rightarrow V4$, and a pure feedback (FB) relationship in the opposite direction. Feedforward (FF) projections originate in superficial layers and target layer 4, which then projects to layers 2/3. Feedback (FB) projections arise from infragranular layers and target both supragranular and infragranular layers, avoiding layer 4. The input to V4, receiving both internal and FF input from V1:

$$I_{V4} = J_{V4} r_{V4} + J_{FF} r_{V1} \quad (2.6)$$

$$\mathbf{J}_{FF} = \begin{bmatrix} J_{FF1} & 0 & 0 & 0 \\ 0 & 0 & 0 & 0 \\ 0 & 0 & 0 & 0 \\ 0 & 0 & 0 & 0 \end{bmatrix}$$

The input to V1, receiving both internal and FB input from V4:

$$I_{V1} = J_{V1}r_{V1} + J_{FB}r_{V4} \quad (2.7)$$

$$\mathbf{J}_{FB} = \begin{bmatrix} 0 & 0 & J_{FB1} & 0 \\ 0 & 0 & J_{FB2} & 0 \\ 0 & 0 & J_{FB3} & 0 \\ 0 & 0 & J_{FB4} & 0 \end{bmatrix}$$

Parameter values for the FF and FB projections are $J_{FF1} = 1$, $J_{FB1} = 0.1$, $J_{FB2} = 0.5$, $J_{FB3} = 0.9$, and $J_{FB4} = 0.5$. Other values for the FB projections, in which the ratio FB1/FB3 is higher, have been also explored.[2]

RESULTS

Intralaminar Level

To analyse the behavior of the model at the intralaminar level, the effect of an increase in stimulus contrast on gamma rhythms for layer 2/3 neurons in V1 was simulated and the outcome was compared with experimental observations.[1] The increase in visual contrast was modeled as an increase in input to the excitatory population, reflecting the fact that contrast increases within a neuron's receptive field typically lead to elevated firing rates. As shown in Fig. 2.1, higher contrast values result in stronger gamma rhythms, characterized by a higher gamma peak in the excitatory firing rate power spectrum. [1]

The power spectrum corresponding to spontaneous activity (i.e., zero input) was subtracted from the shown curves to remove the power-law appearance of the spectra while preserving the principled effects of the input. The increase in spectral power is maximized in the 30–60 Hz gamma band. [1] Moreover, a systematic but small movement of the peak of the gamma toward higher frequencies (from around 30 to 40

Hz) with contrast increase has also been found. [1] This frequency shift effect is reproduced by the model.

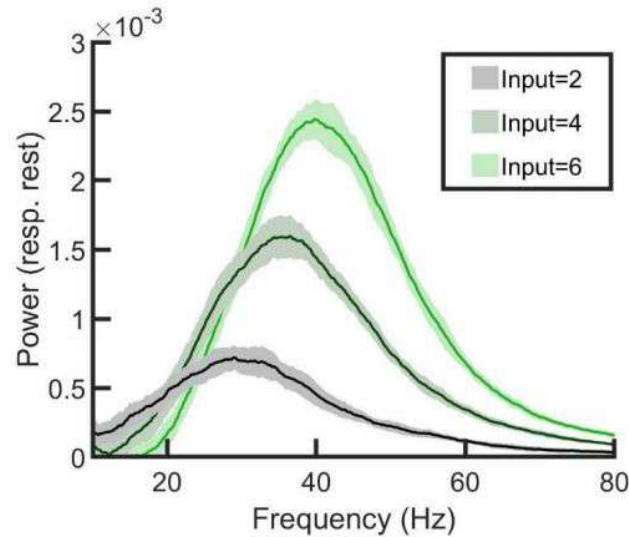


Fig 2.1 Power spectrum of the firing rate of a single layer 2/3 as a function of input strength to the excitatory population. The spontaneous state spectrum (with zero input) has been subtracted in each case to emphasize changes caused by the input (see main text). With increasing input (which is similar to the effect of raising the contrast of a visual stimulus), the power of gamma rhythms increases.[1]

Interlaminar Level

Following the characterization of isolated layer's neural dynamics and the construction of a laminar circuit through interlaminar projections, interplay between alpha and gamma rhythms becomes a target of investigation. The characterization of these interactions provides insight into the coordination of oscillations across layers of cortex.[1]

The alpha-modulated layer 5/6 to layer 2/3 input also significantly influences, causing the entrainment of gamma and alpha rhythms (Fig. 2.2). Here, the slow oscillatory layer 5/6 input modulates the power of layer 2/3 gamma oscillations, leading to a phase-amplitude coupling (PAC) between layer 2/3 gamma and layer 5/6 alpha rhythms. This PAC phenomenon has also been observed in multielectrode recordings in macaques and is a validation of the model at the interlaminar level.[1]

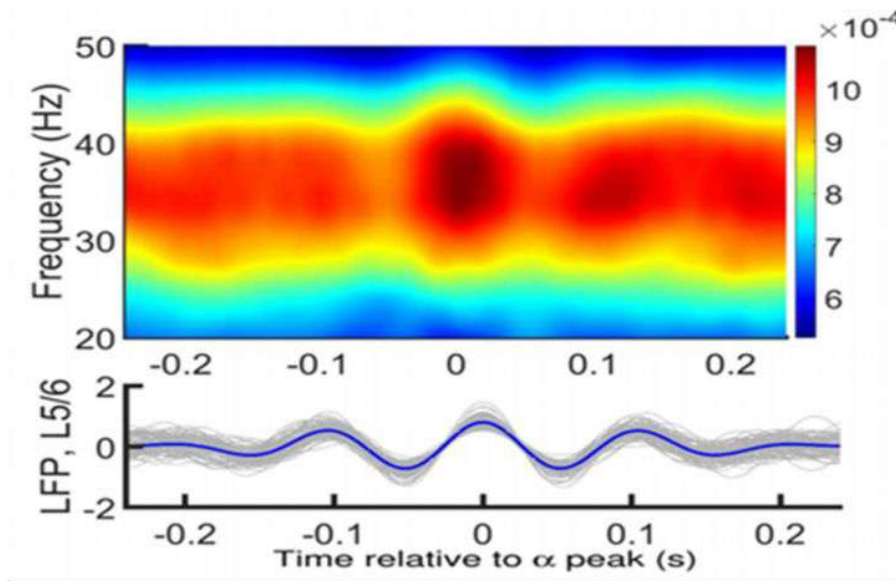


Fig.2.2: Bottom: (.2) ensemble of 30 activity traces in layer 5/6(in Gray) and their mean (in blue). Each trace's central peak was realigned at zero prior to taking the mean. Top: (.2) layer 2/3 periodogram of the averaged power for an interval of frequencies for the same temporal durations as the layer 5/6 traces. The presence of a robust entrainment of gamma power to alpha phase, as in the experimental results Input was $I = 6$ for supragranular and $I = 8$ for infragranular excitatory populations.[1]

Inter-areal interactions

Extrapolating to the interareal level means describing anatomical projections between microcircuits of two or more areas of the cortex. Again, two areas with a well-characterized hierarchical relationship (e.g., areas V1 and V4) are assumed here. FF projections along the visual hierarchy originate from supragranular layers and preferentially project to layer 4, which, in turn, projects to layer 2/3 of that area. In contrast, FB projections are from infragranular layers (mainly layer 6) and target supra- and infragranular layers but not directly layer 4. More recent evidence shows that FB projections from these layers are more diffuse than FF projections as targets. Interareal interactions within the visual areas have been examined in recent studies in the framework of visual attention. Employing a model of two multilaminar regions, the interactions are able to be investigated, and the mechanisms behind them investigated.[1]

Injecting current into V1 excitatory cells caused a significantly increased gamma power in V4 layer 2/3 (Fig. 2.3) and a small, nonsignificant reduction in alpha power in V4 layer 5/6 (Fig. 2.4). This gamma augmentation is accounted for by two considerations: (i) the additional input that comes to V4 layer 2/3 produces a

mean-driven augmentation of gamma power in accordance with what has been found within the local circuit, and (ii) gamma modulation of incoming input further reinforces the intrinsic V4 gamma rhythm through interareal synchronization.[1]

Supercritical injection of current into excitatory cells of V4 produced a dramatic fall in V1 layer 2/3 gamma power and significant and strong induction of V1 layer 5/6 alpha power (Fig. 2.5 and Fig. 2.6). This implies that strong alpha oscillations correspond to FB interactions, with the suppression of the gamma rhythm. [1]

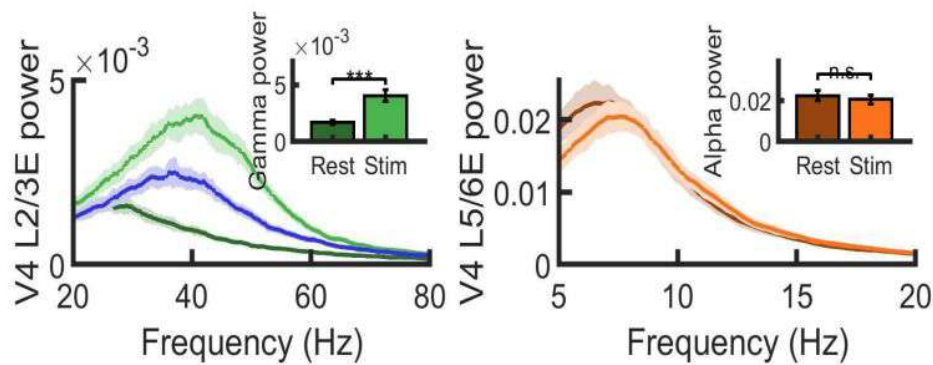


Fig.2.3 and .2.4: Power spectrum at V4 measured at layer 2/3 (.3) and layer 5/6 (.4) for resting and stimulation conditions. Insets represent peak value of the power spectrum at supragranular (.3) and infragranular (.4) layers for identical resting and stimulation conditions. One finds a considerable rise in gamma power, similar to the case of micro stimulation experiments [1]

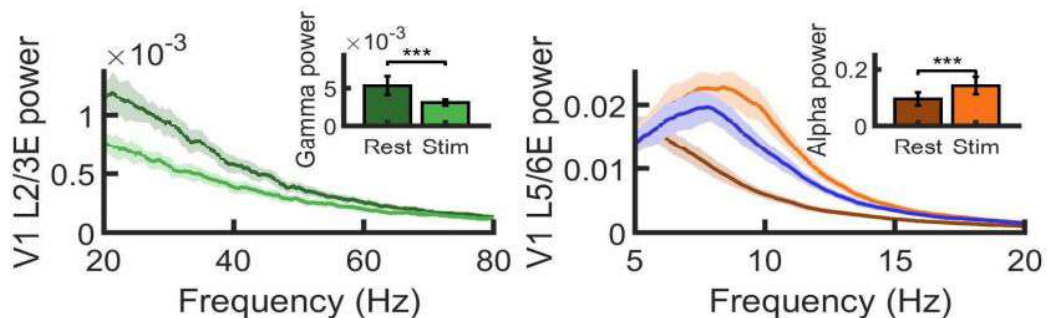


Fig.2.5 and .2.6: Power spectrum in layer 2/3 of V1 (.5) and layer 5/6 (.6) under resting and stimulation conditions. Inset: peak value of power spectrum under these conditions. Strong alpha increase and

gamma reduction were seen as reported experimentally. For (.3) and (.6), blue curve: an isolated piece that gets the same input as in the case of stimulation but without its rhythmic part.[1]

CHAPTER.3

EFFECTS OF ELECTROMAGNETIC FIELD ON THE NEURONAL BEHAVIOUR

INTRODUCTION

Electromagnetic fields (EMF) are a union of electric and magnetic force fields. They are wave-like traveling fields that provide forces to every charged object around them. Many electronic products have been discovered and utilized these days; hence we have been easily exposed to the produced artificial electromagnetic waves in our everyday life. Explosive application of a number of electronic devices in contemporary society has necessarily resulted in continually enhance the possibility of electromagnetic wave exposure. Wireless communication technologies, including computers and mobile phones, have become an indispensable part of contemporary people. As a result, all living organisms on Earth are undergoing environmental alterations and are being subjected to artificial electromagnetic waves which have never been encountered before. The impact of EMF on body systems may be dependent on the frequency, intensity and power of radiation. Multiple studies have revealed that the nervous system is a significant target organ system responsive to EMF. [13]

EMFs may induce both structural and functional alterations in the nervous system. They affect the metabolism and transport of neurotransmitters; for example, in action potentials, transmitter release in synaptic endings is controlled by calcium ion channels. The transmitters diffuse across the synaptic cleft and bind to specific receptors on postsynaptic neurons or effector cells. Neurons exhibit a wide variety of dynamic behaviors resting states, spikes, bursts, and multistability which are all responsive to ion flow rate, transmission delay, external currents, and EMF interference. The Wilson-Cowan model of excitatory and inhibitory neuronal population interactions provides a strong basis on which to examine population-level neural activity under such conditions [2]. By adding a memristive component to this model, electromagnetic induction effects can be simulated by linking changes in membrane potential to electrical behavior based on memory [3]. The Wilson-Cowan model with a memristor displays complex electrical behavior, including asymmetric coexisting states and antimonotonicity effects. These are parameter- and initial condition-dependent phenomena that have been verified using analog circuits built from discrete components [10].

Based on the electromagnetic field theory, the significant effect of electromagnetic radiation can be defined with magnetic flux. The coupling between magnetic flux and membrane potential influences network behavior. Keeping these points in mind,

memristor-based models were designed. Experimental findings done on humans and animals placed in two sources of electromagnetic field (i) Extremely low frequency electromagnetic field (ELF-EF) generally emitted by electric and electronic appliances (ii) Radio frequency magnetic fields (RF-MF) emitted by wireless communication devices like mobile and towers of transmission. [13]. Preparatory to considering the influence of the electromagnetic field on neurons is an explanation of memristor which provides an efficient means of deciphering the change taking place.

MEMRISTOR

A memristor, or "memory resistor," is a special electrical device that has a memory of the charge that has flowed through it. Theoretically, in 1971, by Leon Chua, the memristor was put forth as the fourth basic passive circuit element, joining the resistor, capacitor, and inductor. Unlike other components, the memristor connects electric charge and magnetic flux, and its resistance adjusts based on its current history of what has traveled through it. Because it is capable of storing information about the voltages to which it's been subjected previously, it makes it a favorite for the dramatic revolution that might happen in electronics and computing.

A major characteristic of a memristor is the capability to adapt its resistance by direction and strength of current. As current moves in one direction, resistance rises; when it is moving in the other direction, resistance falls. After the current has ceased, the memristor holds the last resistance level, essentially "remembering" the previous voltage input. Such an effect is often realized by means of thin layers of material such as titanium dioxide, wherein ions with charges modify the resistance. In non-volatile memory devices, memristors retain data when power is eliminated, providing for faster speed and greater density over conventional flash memory.

In neuromorphic computation, memristors replicate synapse behavior of the human brain, providing low-energy, parallel processing and learning. Their unidimensional design also enables very compact circuit forms, which has the potential for creating smaller but more powerful electronics. It is one of the four fundamental passive electrical components, the others being the resistor, the capacitor, and the inductor. [11]

Figure below (**Fig .3.1**) shows a memristive system and symbol of a memristor.

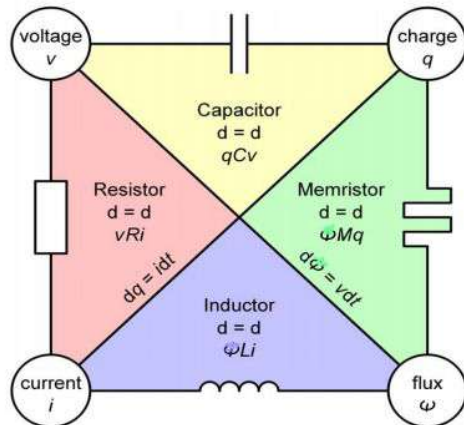


Fig .3.1

In the relationship between magnetic flux linkage ψ_m and electric charge q , the derivative of one with respect to the other depends on the value of one or the other, and so each memristor is characterized by its memristance function describing the charge-dependent rate of change of flux with charge.

$$M(q) = d\psi_m / dq$$

$$M(qt) = (d\psi_m / dt) / (dq/dt) \quad (3.1)$$

$$= V(t) / I(t)$$

This equation reveals that memristance defines a linear relationship between current and voltage, as long as M does not vary with charge. It can be inferred from this that memristance is charge-dependent resistance. If $M(q(t))$ is a constant, then we obtain Ohm's law $R(t) = V(t) / I(t)$.

Memristor properties cannot be achieved by any combination of the other basic components, unites a memory that persists with electrical resistance. That is, a memristor possesses a resistance that "remembers" its previous value when the current was last switched on, so theoretically, it can be employed in the construction of solid-state devices for storing data without needing a constant flow of energy to retain their current values.

They consume less energy and are quicker than current solid-state storage technology and they can store at least double the amount of data in the same space. Memristors are almost radiation-proof, and radiation can interfere with transistor-based technologies. In addition, memristors can make computers that start and stop like a light switch. It was only nearly 40 years later that the first real device was built. This was in 2008, when a team led by Stanley Williams at HP Research Labs came to

understand that switching of the resistance between a conducting and less conducting state in metal-oxide thin-film devices was exhibiting Leon Chua's memristor behavior. The most popular structure of a memristor is a sandwich made up of metal/insulator/metal layers. The conductance of the memristor grows under the action of the applied voltage is the SET process, whereas the conductance diminishes under the action of reversed voltage is referred to as the RESET process. Bipolar and unipolar resistive switching devices are classified according to the polarity of the switching voltage and divide memristors into two groups. Bipolar resistive switching direction depends upon the polarity of the applied voltage, whereas unipolar resistive switching direction depends solely upon the applied voltage.[11]

In recent years, with the gradual improvement in the preparation and performance of memristors, the research focus has shifted from the preparation of devices to the development of artificial intelligence systems, neuromorphic devices and brain-like chips. A diffusion dynamics-based memristor has been constructed, in which the dynamic process of Ag nanoparticles doped into the oxide dielectric layer is identical to the biodynamics of Ca^{+} ions in chemical synapses, indicating that this memristor can naturally simulate bio-synaptic behaviors. On the basis of the synaptic characteristics, artificial nociceptors and artificial sensory alarm systems can be also constructed and designed using diffusion-type memristors. Memristor devices thus hold a lot of potential for use in neuromorphic systems, some of which include memristor-based neural networks.

MEMRISTOR BASED NEURAL NETWORK

Employing memristors to mimic synapses is regarded as one of the most important steps towards the construction of artificial neural networks. A neural network system that consists of about 10¹¹ neurons and 10¹⁵ synapses can handle a vast amount of information with extremely low power consumption. The memristive device possesses extremely high stack density, and the switching speed can be extremely fast, it requires only a small amount of energy and can be made in a smaller size. The memristor possesses tremendous advantages over conventional devices employed in the construction of neural networks. The memristor resistive switching characteristics are of two types: analog type and digital type. Among them, the resistive state of the analog-type memristor is continuous and its conductance can be smoothly varied through electrical pulses, which can be employed to model the continuous variation of bio-synaptic weights and bio-neuronal membrane potential due to external stimulation.

The resistive states of the digital type memristor, however, are discrete in the scanning of the voltage switched between low and high resistive states. As a kind of two-terminal device, the memristor possesses the same structure as the neural synapse (Fig 3.2). The memristor can be miniaturized to the nanometer scale, and the integrated array density can even be the density of bio-synapses in the brain, thus giving the memristor a significant advantage in neural network design. Synapse facilitates behavioral

adjustments and signaling through the movement of Ca^{2+} ions and K^+ ions. To date, electrical conductivity modification in most memristors results from ion movement.[11]

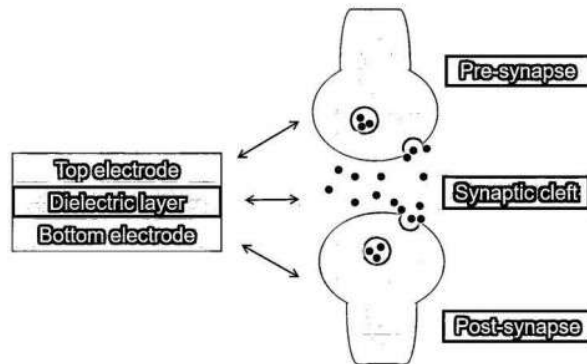


Fig .3.2

Spiking neural network

The SNN introduces randomness into the network neurons, it is closer to bio-neural networks, and its model is more complex and changeable. In an SNN, neurons fire constantly, and both synapses and neurons hold internal states. Normally, the state change within the neuron is described using a differential equation. The impulses that are fed into the neurons can cause the membrane potential to increase or decrease, thus mimicking the excitation and inhibition of synapses. The SNN can also achieve the simulation of analog and digital circuits. During the implementation of analog circuits, the SNN can simulate the brain's dynamics directly, which is helpful to get a better response time, and then combine with additional neurons and synapses. In digital circuit realization, the SNN can be reprogrammed and reconfigured online to further realize high accuracy and robust noise immunity.

The SNN possesses numerous internal variables and intricate connections; therefore, it must consume more computing resources and energy than the DNN.[11]

Artificial neural networks

The ANN is an artificial intelligence computational model and a model based on the bio-neural network. The artificial neurons communicate via artificial synapses, while the neural messages are passed from a neuron to other neurons. ANNs are capable of emulating bio-neural networks' functions, for example, associative memory, conditioned reflexes, and visual recognition. The working mechanism of the neural network includes two: one is the inference and the other is the training. Typically, a loss function is built to describe the degree of convergence of the model in the training process.[11]

Deep neural network

The DNN is one type of multilayer neural network using artificial neurons, that is, deep learning. The DNN tends to use a fairly simple model of the neuron, where the neurons are independent of time during usage, and the neural information propagates from the input layer to the output layer in a numerical form. Layering is a characteristic of DNN, where neurons belonging to the same layer are not networked with one another, but neurons belonging to different layers are networked together via synapses. A DNN is achieved by interlinking numerous layers of such neural networks. The distinguishing characteristic of DNNs is the presence of a high number of layers. In contrast to neural networks with fewer layers, DNNs carry out complicated nonlinear mapping of input samples in order to pull out more abstract concepts, which is crucial to the deployment of artificial intelligence.[11]

Convolutional neural network.

CNN has been utilized in other fields, like image processing and image recognition. CNN is a feedforward neural network with deep structure and convolutional processing, which is one of the standard algorithms in deep learning. A typical CNN is typically made up of a convolution layer, activation layer, normalization layer, pooling layer and full connection layer. As a typical model of deep learning, CNNs occupy an indispensable position in computer vision applications. CNNs can implicitly learn from data and automatically extract features in image processing. Reducing latency, power consumption, and saving energy are the primary difficulties in deploying CNNs in embedded terminals these days.[11]

TiOx - BASED MEMRISTOR

The fabrication of memristors using thin titanium oxide (TiOx) films as a functional layer has been a significant achievement, with research focusing on memory characteristics. TiOx is multi-functional polycrystalline, has wide applications according to its chemical and physical properties. The high photocatalytic activity is a notable physical characteristic of TiOx. A TiOx layer was deposited by magnetron sputtering onto an indium tin oxide (ITO) substrate as a functional layer of the memristive device. Through a comprehensive analysis of conductance on the curves of current–voltage (I-V), a physical model was proposed as plausible to explain the resistive switching (RS) mechanisms based on the space charge-limited current (SCLC) mechanism and Ohmic conduction. The fabricated Ag/TiOx/ITO device has excellent memristive execution and could enhance RS memory behavior. Additionally, this will pave the way for future advancements in device construction and the application of memory devices.[12]

MEMRISTOR CROSS-BAR ARRAY FABRICATION

A crossbar is fabricated using a set of perpendicular nanoscale wires in two layers [10], with a memristor placed at each junction as shown in (Fig 3.3). Due to the non-volatile nature of memristor, the crossbar can be used as a storage unit, where information is stored in the cells as resistance values.[12]

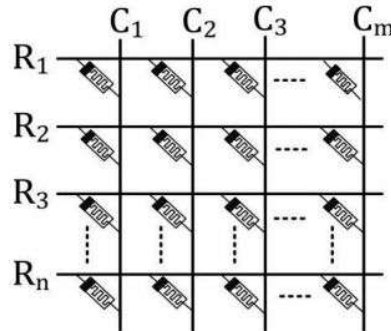


Fig .3.3

For this purpose, this architecture is often referred to as resistive random-access memory (ReRAM). Resistive random-access memory (ReRAM) systems provide mechanism to reduce this bottleneck. Although a number of technologies exist to realize ReRAM systems, memristor is considered to be one of the most suitable candidates due to its non-volatile nature, in-memory computing capability, low power consumption, dense layout, and higher write endurance. In addition to being used as resistive memory, the crossbar can also be used to carry out logic operations. This requires us to apply suitable voltages to the rows and the columns of the crossbar in proper sequence. Essentially, this introduces a new architecture where storage and computation can be carried out in the same hardware. This is often referred to as in-memory (in-situ) computing architecture.

MEMRISTIVE NEURONS

Neuronal functions are often higher in complexity to efficiently perform temporal processing of information. IF (integrated and fire) models are mainly used to realize this simple neuronal function without the decay of membrane potential over time. This model is the simplest of all neuron models that lower computational requirements are required compared to other models. The IF behavior is emulated by a strong nonlinear transition in memristors, like the abrupt increase in conductance in memristive devices. In computational neuroscience, the LIF (leaky integrate-and-fire) neuron model has been developed to enhance the model's bio plausible, after combining the IF neuron with leakage of membrane potential. Currently, LIF models are more prevalent in bio-inspired computing systems with computational efficiency. One of the methods for the

solution to achieve the LIF neuron is using the volatile TS (threshold switching) memristor connected in series with a series resistor and a parallel capacitor. In other memristive devices with volatile effect but no clear threshold switching value, LIF neurons are also feasible. The artificial neurons exhibit high spatiotemporal uniformity and have been utilized to develop neuromorphic hardware that can process sequential data.[13]

MEMRISTIVE WILSON COWAN MODEL

We can modify the Wilson Cowan model by including a memristive term in the equation:

$$\tau_E \frac{dr_E}{dt} = -r_E + \Phi(I_E^{net} + I_E^{ext}) + \sqrt{\tau_E} \xi_E(t) + k(1 - 3|\psi|)r_E \quad (3.2)$$

$$\tau_I \frac{dr_I}{dt} = -r_I + \Phi(I_I^{net} + I_I^{ext}) + \sqrt{\tau_I} \xi_I(t) + k(1 - 3|\psi|)r_E \quad (3.3)$$

Where,

$$\frac{d\psi}{d\tau} = \frac{1}{\tau_\psi} (r_E - \psi) \quad (3.4)$$

Where, k and τ_ψ are two adjustable parameters.

The initial condition values of these two parameters for stimulation are:

$$K = 8.5$$

$$\tau_\psi = 0.7$$

Based on the above extended Wilson cowan model we can understand the effect of electromagnetic field by modifying the results in CHAPTER. 2

Intralaminar Level

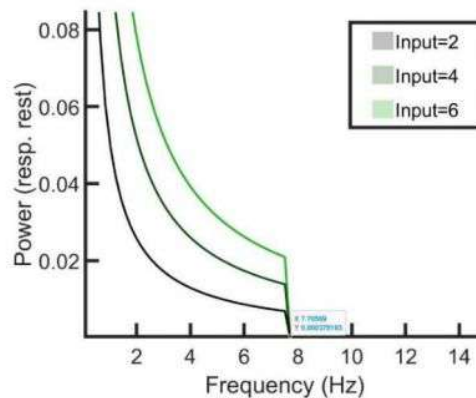


Fig .3.4

For all the inputs, the power spectrum is showing an exponential decrease followed by a drop to zero. This can be interpreted as reflecting the temporal and spatial structure of neural dynamics and the limitations of measurement or system behaviour.

Exponential decrease in the power spectrum suggests that there is a dominance of low frequency components in the neural signals. When electromagnetic effect from the memristor is applied, the brain tends to operate with more power in slower rhythms (delta, theta, alpha bands), which relate to broad coordination and integration of activity across brain areas.

Higher frequencies are less coherent and more noise-like. As frequency increases, the power decreases exponentially, which is common in systems with scale-invariant or self-organized behaviour, such as $1/f$ -like (pink noise) processes often found in EEG data.

Since our studies are limited to theoretical part only, the above-mentioned damping-like behaviour may be an indication of a biophysical constraint, like the low-pass filtering properties of membranes, synapses, or networks. These structures tend to smooth out fast changes in voltage, damping high frequencies.

The sharp drop to zero for all inputs can mean errors in the signal processing artifacts. Since the spectrum is computed with techniques like a windowed FFT and filtering, a sharp drop could result from preprocessing, like applying a low-pass filter or using too short a window.

So, we may conclude that though there is a shortfall in the selection of proper FFT parameters, the exponential decay indicates that when an electromagnetic field is applied, it generates low-frequency, coherent rhythms; high frequencies are less structured.

Interlaminar Level

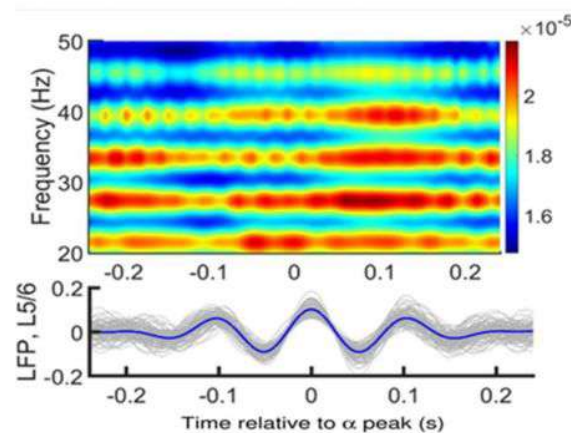


Fig .3.5

Bottom: Set of 30 traces of activity in layer 5/6 (in Gray) and their average (in blue) under the effect of electromagnetic radiation from the memristor. The central peak of each trace was aligned at zero before averaging. Top: Periodogram of layer 2/3 showing the averaged power for a range of frequencies for the same temporal periods as the layer 5/6 traces.

Earlier, as a result of the interlaminar coupling, rhythms spread across layers and the oscillatory dynamics in both supra- and infragranular layers present a more dynamically rich profile, compared to the isolated layers. But the electromagnetic flux from the memristor modulates the power of gamma oscillations in layer 2/3 and the, phase-amplitude coupling (PAC) between layer 2/3 gamma and layer 5/6 alpha rhythms have been disrupted.

Inter-areal interactions

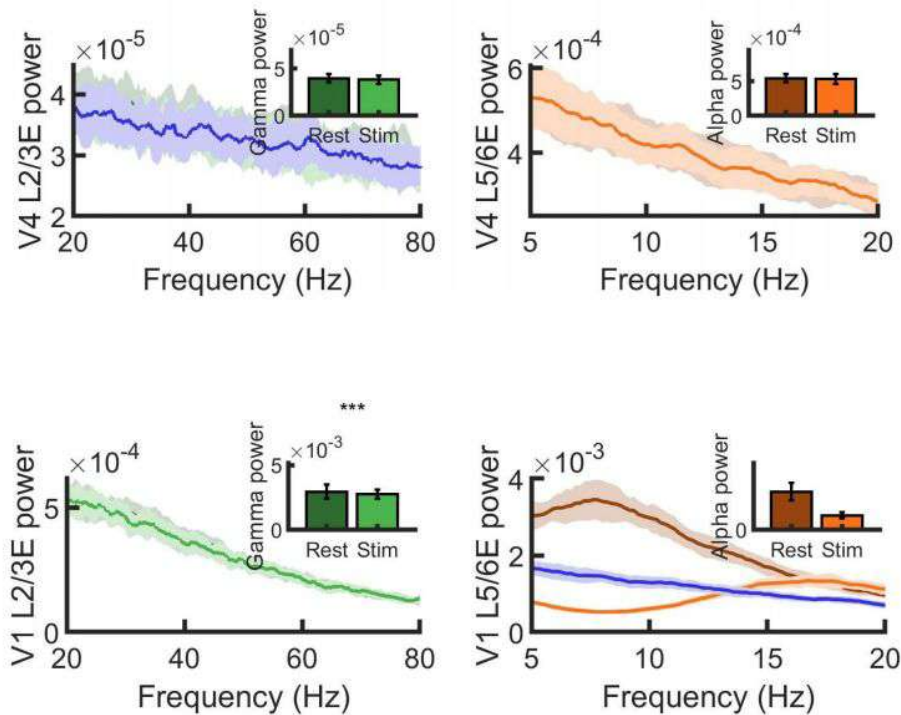


Fig .3.6

Gamma rhythms are not just local markers of excitation, but also carry signatures of interareal connectivity and synchronization. But when the electromagnetic flux is added to the input, the synchronization has been increased between resting and stimulated values. It should also be noted that the magnitude of the power has been significantly reduced in accordance with the results as seen from Fig. 3

Alpha rhythms have become significant as more power is distributed among lower frequencies.

Conclusion

Alpha and gamma rhythms, two of the most studied brain oscillations, are thought to serve very different but complementary roles in neural processing.

Gamma Rhythms are usually associated with Feedforward (FF) communication between cortical areas, local computation — e.g., encoding sensory input, feature binding and also attention, perception, and working memory. Gamma is often seen as a marker of active processing — when neurons are engaged and passing along precise information.

Alpha Rhythms (~8–12 Hz) are associated with Feedback (FB) communication, especially from higher-order to lower-order areas, Inhibition or suppression of irrelevant or distracting inputs and Internal states, like relaxed wakefulness or disengagement from external input.

Alpha is thought to reflect a gating mechanism — it modulates cortical excitability, essentially tuning the "volume" of brain areas. It is often linked to top-down control, like directing attention or expectation.

When we modulated the neuronal dynamics with the external electromagnetic flux from the memristor, an Alpha–Gamma interplay is seen. This interplay allows for selective routing of information — gamma transmits content, alpha controls when and where that content flows.

Hence it is evident that the external electromagnetic perturbation definitely changes how the neuronal firing happens, it also alters the timing and frequency of the neuronal bursts.

Though the study is limited to formulating the governing equations under external effects and simulating the results, we hope that it will pave path for future studies in determining the interconnection between external electromagnetic stimuli and brain function.

References

1. Feedforward and feedback frequency-dependent interactions in a large-scale laminar network of the primate cortex Jorge F. Mejias, John D. Murray, Henry Kennedy, Xiao-Jing Wang.
2. Supplementary Materials for Feedforward and feedback frequency-dependent interactions in a largescale laminar network of the primate cortex Jorge F. Mejias, John D. Murray, Henry Kennedy, Xiao-Jing Wang.
3. Theoretical Neuroscience: Computational and Mathematical modeling for neural systems. Dayan, P., & Abbott, L. F. (2001).
4. Principles of Neural Science. Kandel, E. R., et al. (2013).
5. Principles of Neural Coding. Quiroga, R. Q., & Panzeri, S. (2013).
6. Spiking Neuron Models. Gerstner, W., & Kistler, W. M. (2002).
7. Excitatory and inhibitory interactions in localized populations of model neurons. Wilson, H.R., & Cowan, J.D. (1972). Biophysical Journal.
8. Memristor—The missing circuit element. IEEE Transactions on Circuit Theory, Chua, L.O. (1971).
9. Rich dynamics in a new memristive Wilson-Cowan neural network and circuit implementation. Nonlinear Dynamics, Bao, B.C., & Xu, Y.H. (2019).
10. Foundations of Mathematical Neuroscience - Bard Ermentrout & David Terman
11. Memristor-based neural networks: a bridge from device to artificial intelligence - Zelin Cao, Bai Sun, Guangdong Zhou, Shuangsoo Mao, Shouhui Zhu, Jie Zhang, Chuan Ke, Yong Zhaodef and Jinyou Shao
12. Experimental demonstration of highly reliable dynamic memristor for artificial neuron and neuromorphic computing. - See-On Park, Hakcheon Jeong, Jongyong Park, Jongmin Bae & Shinhyun Choi.
13. Emerging memristive neurons for neuromorphic computing and sensing - Zhiyuan Li, Wei Tang, Beining Zhang, Rui Yang & Xiangshui Miao.
14. Possible Effects of Radiofrequency Electromagnetic Field Exposure on Central Nerve System - Ju Hwan Kim, Jin-Koo Lee, Hyung-Gun Kim, Kyu-Bong Kim and Hak Rim Kim.

15. Electromagnetic induction effects on electrical activity within a memristive Wilson neuron model Quan Xu, Zhutao Ju, Shoukui Ding, Chengtao Feng, MoChen, Bocheng Bao.
16. Modified Morris-Lecar neuron model: Effects of very low frequency electric fields and of magnetic fields on the local and network dynamics of an excitable media - Karthikeyan Rajagopal, Irene Moroz, Balamurali Ramakrishnan, Anitha Karthikeyn, Prakash Duraisamy.
17. Engagement of Pulvino-cortical Feedforward and Feedback Pathways in Cognitive Computations Jorge Jaramillo, Jorge F. Mejias, Xiao-Jing Wang.